

# Direct Evidence of a Near-Ideal $J_{\text{eff}} = 1/2$ Ground State in Triangular-Lattice $\text{Na}_2\text{BaCo}(\text{PO}_4)_2$

M. M. Ferreira-Carvalho,<sup>1,2</sup> S.H. Chen,<sup>1</sup> Y. C. Ku,<sup>3,4</sup> Anagha Jose,<sup>5</sup> Ryan Morrow,<sup>5</sup> C. Y. Kuo,<sup>3,4</sup> C. F. Chang,<sup>1</sup> Z. Hu,<sup>1</sup> M. W. Haverkort,<sup>6</sup> and L. H. Tjeng<sup>1</sup>

<sup>1</sup>Max Planck Institute for Chemical Physics of Solids, Nöthnitzer Str. 40, 01187 Dresden, Germany

<sup>2</sup>Institute of Physics II, University of Cologne, Zülpicher Straße 77, 50937 Cologne, Germany

<sup>3</sup>Department of Electrophysics, National Yang Ming Chiao Tung University, Hsinchu, Taiwan

<sup>4</sup>National Synchrotron Radiation Research Center, Hsinchu, Taiwan

<sup>5</sup>Institut für Festkörperphysik, Leibniz IFW Dresden, D-01069 Dresden, Germany

<sup>6</sup>Institute for theoretical physics, Heidelberg University, Philosophenweg 19, 69120 Heidelberg, Germany

(Dated: February 10, 2026)

We investigated the local Co 3d electronic structure of  $\text{Na}_2\text{BaCo}(\text{PO}_4)_2$  using polarization-dependent X-ray absorption spectroscopy (XAS) in combination with full multiplet cluster calculations. We employed the line-fitting inverse partial fluorescence yield (IPFY) technique to obtain accurate XAS spectra from strong insulating materials. Our combined experimental and theoretical analysis reveals a very small effective trigonal distortion of only 11 meV in the  $\text{CoO}_6$  octahedra, indicating a close to ideal condition to render a ground state with the  $J_{\text{eff}} = 1/2$  character. With our cluster model we were also able to simulate magnetic susceptibility measurements along different directions in the crystal. These findings highlight  $\text{Na}_2\text{BaCo}(\text{PO}_4)_2$  as a promising platform for exploring exotic magnetic phenomena associated with  $J_{\text{eff}} = 1/2$  ground states on triangular lattices.

## I. INTRODUCTION

Frustrated quantum magnets provide a rich platform for exploring unconventional quantum phases driven by competing interactions and reduced dimensionality. Among these, two-dimensional  $S = 1/2$  triangular lattices have been the focus of many theoretical and experimental studies of frustration-induced phenomena [1–3]. In such systems, geometric frustration and quantum fluctuations act together to destabilize conventional magnetic order, enabling the possibility of exotic ground states. While early theoretical work showed that the  $S = 1/2$  Heisenberg antiferromagnets on a triangular lattice exhibits a  $120^\circ$  non-collinear ordered state [4–7], later studies demonstrated that long-range order can be suppressed through extended exchange interactions, with emerging anisotropic interactions [8–16].

Recently, triangular-lattice cobaltates with  $\text{Co}^{2+}$  ions in octahedral coordination have attracted strong interest due to their interplay of frustration and spin orbit coupling (SOC) [17]. In these  $d^7$  systems, crystal field effects and SOC can stabilize a well-isolated, Kramers-degenerate  $J_{\text{eff}} = 1/2$  ground state. This pseudospin state in a triangular lattice creates an ideal environment for studying potential emergent quantum phases.

In this study we investigate  $\text{Na}_2\text{BaCo}(\text{PO}_4)_2$ . Figure 1 (a) and (b) display the  $Pm\bar{3}1$  structure crystal structure and the triangular lattice arrangement of the Co ions in the  $ab$  plane. This compound has been recently the subject of intense and conflicting research, reflecting the complexity of its magnetic ground state. Early debates centered on the presence or absence of long-range magnetic order, with several studies supporting the emergence of a quantum spin liquid (QSL) phase. These include an initially reported exceptionally low ordering

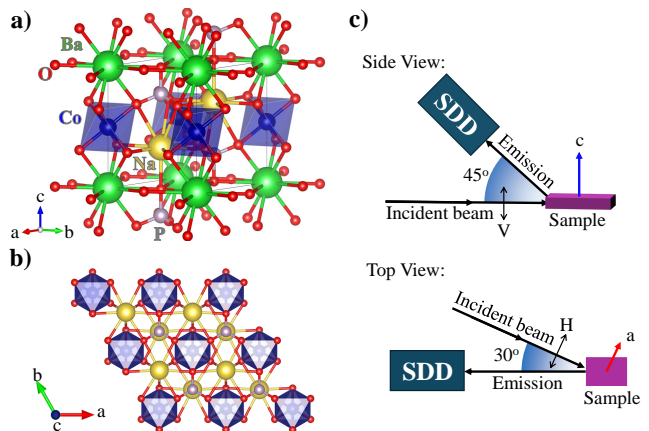


FIG. 1. (a) Crystal structure of  $\text{Na}_2\text{BaCo}(\text{PO}_4)_2$ , showing layers of  $\text{CoO}_6$  octahedra stacked along the  $c$ -axis. (b) The  $ab$  plane containing the  $\text{Co}^{2+}$  triangular lattice. (c) Schematic of the experimental geometry, illustrating the orientation of the incident X-ray beam, linear polarization directions, and the silicon drift detector (SDD) relative to the sample.

temperature of approximately 50 mK [18], later revised to around 148 mK alongside evidence of a nonzero residual thermal conductivity [19], as well as the observation of spinon-like excitations [20].

However, other studies have presented less compelling evidence for a QSL, pointing instead to more conventional magnetic behavior [21–23]. More recently, the focus has shifted to consider this material as a promising candidate for the realization of the long-sought spin-supersolid state [24, 25].

The core of this ongoing debate lies in the details of the interplay between geometric frustration and strong

SOC. The delicate balance is highly sensitive to small changes in local structure or interactions. To clarify the microscopic origin of unconventional magnetism and to assess its suitability as a Kitaev/spin-liquid system, a direct local probe of the local  $\text{Co}^{2+}$  electronic structure is necessary. It is known that  $\text{Co } d^7$  in octahedral coordination displays low lying excited states that are easily populated with increasing temperature, rendering Curie-Weiss fit of magnetic susceptibility not reliable for the determination of ground state properties [26]. It is also important to note that a distortion of the  $\text{CoO}_6$  octahedra has a strong impact on the electronic properties. There is however confusion in the literature about the sign of the trigonal distortion, i.e. whether the  $t_{2g}$  hole is more in the  $e_g^\pi$  or in the  $a_{1g}$  orbital [27–30].

Here, we report on our experimental study on  $\text{Na}_2\text{BaCo}(\text{PO}_4)_2$  single crystals using polarization dependent soft X-ray absorption spectroscopy (XAS) at the  $\text{Co } L_{2,3}$  edge, an element specific technique which is inherently sensitive to the local  $\text{Co } 3d$  electronic structure. Importantly, dipole selection rules govern the accessibility and intensity of distinct final states, making XAS a powerful probe of the ground state and low-lying excited states when combined with theoretical calculations. XAS is a high-energy spectroscopic technique and can determine the interaction parameters like crystal fields, covalency, SOC, and local distortions that build up the low energy excitations [26, 31–35]. For our  $\text{Co}^{2+}$  case, the technique is extremely sensitive to which of the lowest  $J_{\text{eff}} = \frac{1}{2}, \frac{3}{2}$ , or  $\frac{5}{2}$  states are occupied and by using the temperature dependence it provides access to the excited states. The polarization dependence is in particular powerful to shed light on the symmetry and magnitude of the non-octahedral local distortion and the resulting  $3d$  orbital occupation.

Such soft XAS measurements can be challenging, owing to the fact that insulating samples prove to be non-ideal for acquisition of reliable data due to charging effects in the commonly used total electron yield mode, or due to self absorption effects in the total fluorescence yield mode. In order to overcome such limitations but still make use of the strengths of the technique, we employed inverse partial fluorescence yield method [36, 37], which is bulk sensitive and not prone to charging or self absorption effects. To obtain the desired information concerning the local  $\text{Co } d$  quantum numbers, we performed a theoretical analysis of the measured spectra using configuration interaction cluster calculations. Furthermore, the CI-derived ground state, low-lying excited states, and their energy splittings reproduce the measured temperature-dependent susceptibility, confirming the internal consistency of these parameters.

## II. METHODS

Single crystals of  $\text{Na}_2\text{BaCo}(\text{PO}_4)_2$  were prepared from stoichiometric amounts of  $(\text{NH}_4)_2\text{HPO}_4$ ,  $\text{BaCO}_3$ ,

$\text{Na}_2\text{CO}_3$ , and  $\text{CoCO}_3$ , with additional  $\text{NaCl}$  added as a flux. The mixture was thoroughly ground and heat-treated in an  $\text{Al}_2\text{O}_3$  crucible using a box furnace. It was heated to  $950^\circ\text{C}$  and then slowly cooled to  $750^\circ\text{C}$  at a rate of  $3^\circ\text{C}/\text{h}$ . Pinkish, transparent thin-plate crystals were obtained with typical dimensions of  $2 \times 3 \text{ mm}^2$  in-plane and  $\sim 0.1 \text{ mm}$  thickness, consistent with a highly insulating, layered material.

The XAS experiment was conducted at beamline TPS 45A1 of the National Synchrotron Radiation Research Center in Taiwan [38]. The experimental geometry is illustrated in Figure 1 (c). The  $\text{Na}_2\text{BaCo}(\text{PO}_4)_2$  sample was mounted in an aluminum sample holder and cleaved in a preparation chamber with a base pressure of  $10^{-10} \text{ mbar}$  to obtain a clean surface. It was then transferred in vacuo to the measurement chamber, which had a base pressure of  $10^{-11} \text{ mbar}$ .

During the measurement, the sample was oriented such that the linearly horizontally polarized soft X-rays (LH) polarization was aligned parallel to the  $a$ -axis, while the linearly vertically polarized X-rays (LV) polarization was parallel to the  $c$ -axis. The beam spot size in the vertical direction was set to  $7 \mu\text{m}$  to accommodate the platelet thickness of  $\sim 100 \mu\text{m}$ . A  $\text{CoO}$  reference sample was measured simultaneously upstream of the beam to allow for precise energy calibration. For each scan the incident beam polarization was set to either LH or LV by rotating the polarization of the X-ray beam, allowing the measurement of the linear dichroism (LD) between the in-plane and out of plane directions without changing the beam spot on the sample. The spectra were collected at  $T = 300 \text{ K}, 200 \text{ K}, 100 \text{ K}$  and  $40 \text{ K}$ .

A further improvement of the iPFY technique, namely by line fitting the emission spectra as described in more detail in [39], was used to accurately capture the spectral line shape and relative peak intensities. This improved procedure is necessary in situations where the incident beam energy encompasses absorption edges of elements with emission energies close to the monitored O- $K$  emission, in the present case,  $\text{Ba } M_\alpha$ .

For the simulation of the XAS spectra and magnetic susceptibility, we carried out the well-proven full-multiplet configuration-interaction calculations using a  $\text{CoO}_6$  cluster. It accounts for the intra-atomic  $\text{Co } 3d$ - $3d$  and  $2p$ - $3d$  Coulomb interactions, the atomic  $\text{Co } 2p$  and  $3d$  spin-orbit couplings, the  $\text{O } 2p$  -  $\text{Co } 3d$  hybridization, and the local crystal field [31, 32]. We used the QUANTY code [40–43]. Parameters for the multipole part of the Coulomb interactions and the SOC were given by the Hartree-Fock values [44], while the monopole parts as well as the  $\text{O } 2p$  to  $\text{Co } 3d$  charge transfer energies were estimated from photoemission experiments on typical  $\text{Co}^{2+}$  compounds [45]. The SOC value of 66 meV for the  $\text{Co } 3d^7$  configuration was shown to reproduce well the XAS spectra and ground state properties of  $\text{Co}^{2+}$  oxides [26, 46, 47].

The hybridization parameters for the full-multiplet configuration-interaction cluster calculations were de-

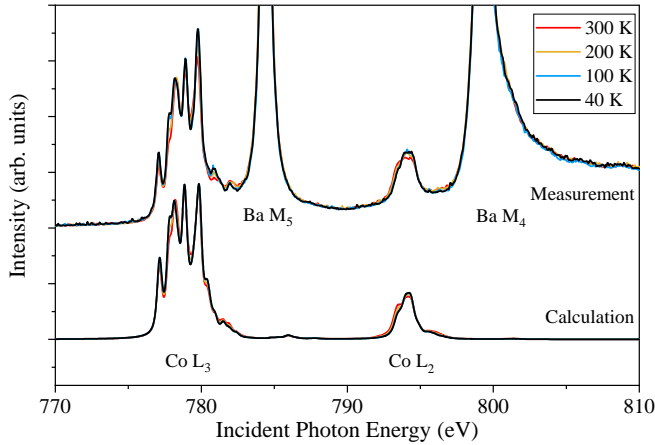


FIG. 2. Experimental and calculated temperature dependence of isotropic spectra measured for  $\text{Na}_2\text{BaCo}(\text{PO}_4)_2$

rived from a tight-binding model constructed from an *ab initio* Wannierized LDA band structure, obtained using the FPLO code [48, 49], and then scaled to fit the experimental data.

Magnetic susceptibility measurements were performed using a Quantum Design MPMS-XL (model CXL398CE) SQUID magnetometer.

### III. X-RAY ABSORPTION

The temperature dependence of the isotropic  $\text{Co } L_{2,3}$  and  $\text{Ba } M_{4,5}$  absorption spectra is presented in figure 2. These spectra were constructed using  $(2 \times I_{\text{LH}} + I_{\text{LV}})/3$ , where  $I_{\text{LH}}$  and  $I_{\text{LV}}$  denote inverse partial fluorescence yield (iPFY) spectra measured using linear horizontal (LH) and linear vertical (LV) polarization, respectively. The observed temperature dependence arises from thermal population of low-lying excited states as temperature increases. This behavior is expected for a high-spin  $\text{Co}^{2+}$  ion in octahedral coordination, where the lowest-energy states are split by 3d SOC of 66 meV. This relatively small energy scale allows for significant thermal population of low-lying excited states with a few hundred Kelvin, leading to the deviation of the Curie Weiss behavior in magnetic susceptibility [26] and the strong temperature dependence of the  $\text{Co } L_{2,3}$  XAS spectra.

The  $\text{Co } L_{2,3}$  spectral shape is governed by a complex multiplet structure resulting from intra-atomic Coulomb interactions, local crystal fields, and hybridization with oxygen ligands. To extract more detailed information on the local electronic structure, we performed multiplet calculations based on a  $\text{CoO}_6$  cluster with  $D_{3d}$  symmetry with the  $C_3$  axis aligned along the  $z$ -direction, consistent with the local Co point group symmetry of  $\bar{3}m$ . Input parameters for the calculations can be found in [50]. We are able to accurately reproduce the spectra and its temperature dependence as shown in figure 2. Our simulations include the full atomic multiplet theory, incorporation

of the  $3d-3d$  and  $2p-3d$  Coulomb interactions, SOC for both  $2p$  and  $3d$  electrons,  $\text{Co } 3d-\text{O } 2p$  hybridization, and ligand crystal fields.

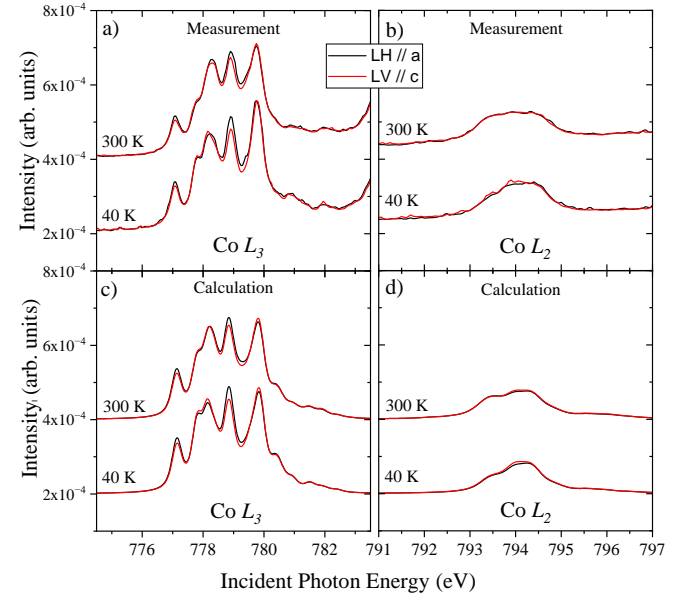


FIG. 3. Polarization-dependent  $\text{Co } L_{2,3}$  XAS spectra taken at 40 K and 300 K: (a,b) experiment and (c,d) calculation. Incident beam polarization is along either  $a$  (LH) or along  $c$  direction (LV).

Figure 3 a) and b) display the polarization-dependent  $\text{Co } L_{2,3}$  XAS spectra taken at 40 K and 300 K. The spectra taken with LV and LH polarizations are almost identical, indicating that the local environment is nearly cubic, close to ideal  $O_h$  symmetry. This is further supported by our simulations, which match the measurements very well as shown in figure 3 c) and d). With the difference between the LV and LH polarizations being so small, we present in figure 4 with an enlarge vertical scale the linear dichroic spectra, defined as the difference between the spectra taken with LV and LH polarizations. We were also able to simulate these LD spectra accurately, including their temperature dependence.

The best fit to the experimental data was achieved using a trigonal distortion parameter of  $D_{\text{trig}} = E_{e_g^\pi} - E_{a_{1g}} = 8 \text{ meV}$ . This value is significantly smaller than the SOC constant energy scale (66 meV), suggesting only minor deviations from a  $J_{\text{eff}} = \frac{1}{2}$  ground state (if only the  $t_{2g}$  orbitals span the Hilbert space, see discussion section below). This agreement between calculation and measurement indicates that the present crystal field and hopping parameters accurately capture the local electronic structure of the  $\text{Co}^{2+}$  ions in  $\text{Na}_2\text{BaCo}(\text{PO}_4)_2$ . Here we note that the positive value of the trigonal distortion is a direct result of the observed polarization dependence of the XAS spectra, namely that the hole density in the  $t_{2g}$  orbital manifold is more in the  $e_g^\pi$  orbitals than in the  $a_{1g}$ . This finding may seem counter intuitive since the refined crystal structure shows a slight elongation

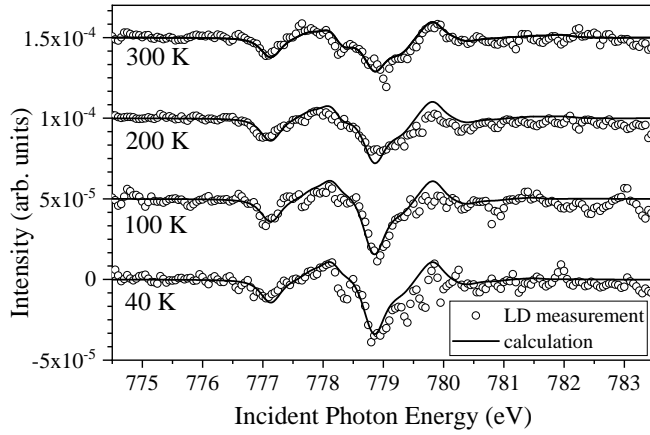


FIG. 4. Temperature dependence of the measured and calculated linear dichroic spectra defined as  $I_{LD} = I_{LV} - I_{LH}$  (see text for definition of the polarizations directions)

along the  $c$ -axis of the local octahedra. However, longer-range interactions apparently contribute as well, thereby reversing the local crystal field scheme, as is the case in, for example, BaCoO<sub>3</sub> [35] and Na<sub>3</sub>Co<sub>2</sub>SbO<sub>6</sub> [51].

#### IV. MAGNETIC SUSCEPTIBILITY

To further check our model, we used the parameters obtained from our XAS analysis [50] to simulate the magnetic susceptibility measurements with the applied field along different directions. Figure 5 shows susceptibility data measured for a 0.1 T field applied along the [001] and [100] directions. The data are normalized to sample weight and applied magnetic field and corrected for diamagnetic contributions following [52]. The experimental susceptibility clearly deviates from ideal Curie–Weiss behavior, as previously explained [26], due to the thermal population of low-lying excited states. We are also able to simulate these curves with our cluster model as shown in figure 5. In order to calculate this temperature dependence, we start with the same parameters used for XAS, but now include the external magnetic field of 0.1 T along the relevant directions ([100] and [001] respectively). We then calculate the expectation values of  $\langle S \rangle$  and  $\langle L \rangle$  for all the states. To calculate the magnetic susceptibility  $\chi(T)$ , at a given temperature  $T$ , we sum the contributions of each state  $i$ , weighted by their thermal occupation:

$$\chi = \frac{M}{H} = - \sum_i \frac{f_i(T) \langle L^{(i)} + 2S^{(i)} \rangle \mu_B}{H_{\text{Tesla}}} \frac{N_A}{10} \quad (1)$$

With  $f_i$  being the Boltzmann distribution for a given temperature  $T$  and  $Z$  the partition sum.

$$f_i(T) = \frac{1}{Z} e^{-E_i/k_B T}, \quad Z = \sum_i e^{-E_i/k_B T}$$

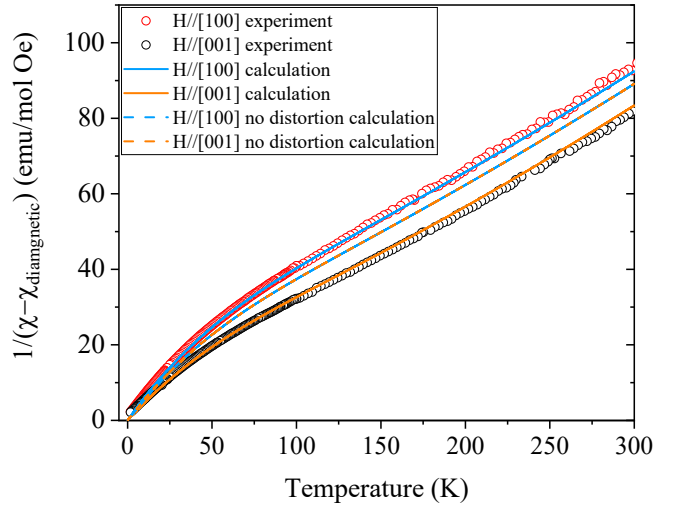


FIG. 5. Inverse magnetic susceptibility,  $\chi^{-1}$ , measured under an applied field of 0.1 T set either along the [100] or [001] crystallographic directions, compared with calculations from our cluster model. Dashed lines indicate simulated susceptibilities obtained without including trigonal distortion in the calculations.

$H_{\text{Tesla}}$  corresponds to the external applied magnetic field. To have the same units as measurement, mol Oe/emu, we multiply by  $\mu_B$ , Bohr magneton, and  $N_A$ , the Avogadro number. The 1/10 factor comes from the conversion from Tesla to Gauss. Figure 5 also highlights the importance of the trigonal distortion parameter in the description of this system. Without this term, the calculated susceptibilities along the two crystallographic directions are identical, in contrast to the experimental results.

A very small antiferromagnetic exchange ( $H_{\text{ex}} = J\langle S \rangle \approx -0.0018$  meV) was applied to match the experiment. This weak exchange term can be interpreted as an emergent local field, generated by short-range antiferromagnetic correlations under the influence of the applied magnetic field. A band structure study based on single-crystal electron spin resonance, powder static magnetization and susceptibility measurements, reports a similarly small, isotropic antiferromagnetic exchange constant of  $J = 0.8\text{--}1.37$  K (approximately 0.068–0.118 meV) [27]. This corroborates the picture of very weak, short-range antiferromagnetic correlations superimposed on the dominant single-ion crystal-field and spin–orbit interactions. Despite its small magnitude, this local field is sufficient to fine-tune the susceptibility curve, especially in the regime where thermal populations of excited states evolve rapidly. Crucially, because  $H_{\text{ex}}$  couples only to the spin component it does not perturb the XAS line-shape. The resulting consistency between spectroscopic and bulk magnetic data therefore highlights the validity of our single-cluster Hamiltonian parameters.

We can estimate effective g factors using the relation  $M = gM_{J_{\text{eff}}}$ , considering  $M_{J_{\text{eff}}} = 1/2$ , to be  $g_a = 4.54$  and  $g_c = 5.18$  (values obtained in a calculation using  $H =$

6 T). Alternatively, using the relation  $\Delta E = g\mu_B B$  where  $\Delta E$  is the splitting of the doublet due to the magnetic field, we obtain  $g_a = 4.30$  and  $g_c = 4.90$ . The latter values are in very good agreement to previously reported values of  $g_a = 4.24$  and  $g_c = 4.83$  [27]. This small anisotropy can be related with the very small trigonal distortion present in the system.

## V. DISCUSSION

Since covalency play a significant role in transition metal oxides, local crystal fields are determined not only by the electrostatic potentials (“ionic” crystal fields) but very much also by the hybridization with the ligands. To determine these “effective” crystal fields, we need to calculate the differences in the total energies of the states of interest with the SOC set to zero. To obtain the effective  $10Dq_{\text{eff}}$ , we first set  $D_{\text{trig}}^{\text{ion}} = 0$  and find the difference in energy between the  $t_{2g}^5 e_g^2$  configuration ground state  $^4T_1$  term with the first excited state corresponding to a  $t_{2g}^4 e_g^3$  configuration  $^4T_2$  term, giving  $10Dq_{\text{eff}} = 0.626$  eV. To determine the effective trigonal distortion we do a similar calculation but this time including  $D_{\text{trig}}^{\text{ion}} = 8$  meV, as found in our experimental fit. When a cubic state is distorted trigonally, the previous  $^4T_1$  ground state term will split into  $^4A$  and  $^4E$  states. The difference between this two states will give the effective trigonal distortion, which for the current set of parameters corresponds to 11 meV. This value is in agreement with a recent Raman study [28] and supports the finding from a band structure study of  $\text{Na}_2\text{BaCo}(\text{PO}_4)_2$  [27]. In our calculations, we obtain a separation between ground state  $J_{\text{eff}} = 1/2$  and first excited state  $J_{\text{eff}} = 3/2$  of about 40 meV. This value explains the excitations found by recent Raman scattering experiments: 39 meV [28] and 38 meV [29].

In our calculations we include the hybridization of the Co  $3d$  with neighbouring O  $2p$  states, resulting in a ground state consisting of the following local configurations:

$$\Psi(\text{Co}^{2+}) = \alpha_7|d^7\rangle + \alpha_8|d^8\underline{L}\rangle + \alpha_9|d^9\underline{L}^2\rangle \quad (2)$$

where  $\underline{L}$  denotes a ligand hole, and  $\sum_{i=7}^9 \alpha_i^2 = 1$ . We obtain the following weights for each configuration:  $\alpha_7^2 = 0.886$ ,  $\alpha_8^2 = 0.112$  and  $\alpha_9^2 = 0.0023$ . We thus have in total 2.88 holes in the  $3d$  shell with a dominant  $d^7$  configuration for the ground state.

The dominant  $d^7$  ground state combined with the very small trigonal distortion further hints that this compound should be very close to ideal  $J_{\text{eff}} = 1/2$  ground state. To quantify this, we computed the expectation value  $\langle \mathbf{J}_{\text{eff}}^2 \rangle$  by constructing the effective total angular momentum operator  $\mathbf{J}_{\text{eff}} = \mathbf{L}_{\text{eff}} + \mathbf{S}$ , where the effective orbital angular momentum operator  $\mathbf{L}_{\text{eff}}$  is obtained by rotating the standard angular momentum operator  $\mathbf{L}$  into the cubic harmonics basis [53]. The rotation matrix

is modified to retain only the  $t_{2g}$  subset of the  $3d$  orbital manifold. After projecting out the  $e_g$  orbitals, the angular momentum operator is then rotated back into the spherical harmonics basis. This total angular momentum operator is then evaluated over the full  $\text{CoO}_6$  cluster to include the effects of Co-O covalency.

It is important to note that a value of  $J_{\text{eff}} = 1/2$  is only obtained when  $t_{2g}$  orbitals fully span the Hilbert space, one can do this by setting  $10Dq$  to a infinitely large value. For example, setting  $10Dq = 10$  eV one finds  $J_{\text{eff}} = 0.501$ . For the found  $10Dq$  crystal field, not in the infinite limit, we obtain  $J_{\text{eff}} = 0.854$ , indicating some participation of  $e_g$  orbitals. Nevertheless, the ground-state remains a well-separated Kramers doublet, preserving its quasi- $J_{\text{eff}} = \frac{1}{2}$  character.

## VI. CONCLUSION

In this work, we have demonstrated that temperature-dependent X-ray absorption spectroscopy offers an exceptionally powerful and precise probe of the local electronic structure in highly insulating transition-metal compounds. By directly measuring the dichroic spectra of  $\text{Na}_2\text{BaCo}(\text{PO}_4)_2$  as a function of temperature, we observe a very small distortion of the  $\text{CoO}_6$  of  $D_{\text{trig}} \approx 11$  meV. We also confirm a  $\text{Co}^{2+}$  valence state, with the predominance of a  $J_{\text{eff}} = \frac{1}{2}$  ground state in  $\text{Na}_2\text{BaCo}(\text{PO}_4)_2$ , with our model also being able to reproduce rather well magnetic susceptibility measurements along different directions, highlighting the local geometric frustration experienced by the  $\text{Co}^{2+}$  ions.

The crystal-field parameters and other relevant electronic structure parameters determined here should provide a solid quantitative foundation for future theoretical descriptions of  $\text{Na}_2\text{BaCo}(\text{PO}_4)_2$  and related two-dimensional  $J_{\text{eff}} = \frac{1}{2}$  triangular-lattice magnets. More broadly, the ability of temperature-dependent XAS to resolve meV scale distortions and orbital occupations offers a powerful toolkit for understanding the microscopic interactions that give rise to unconventional magnetic phenomena in highly frustrated systems.

## ACKNOWLEDGMENTS

M.M.F.-C. greatly acknowledges funding from the Deutsche Forschungsgemeinschaft (DFG, German Research Foundation) Grant No. 387555779. Work at MPI-CPfS Dresden was partially supported by SFB1143 (Project No. 247310070). The authors acknowledge the support from the Max Planck-POSTECH-Hsinchu Center for Complex Phase Materials.

## DATA AVAILABILITY

The data that support the findings of this article are openly available [54].

---

[1] P.W. Anderson. Resonating Valence Bonds: A New Kind of Insulator? *Materials Research Bulletin*, 8(2):153–160, 1973.

[2] A. V. Chubukov and D. I. Golosov. Quantum Theory of an Antiferromagnet on a Triangular Lattice in a Magnetic Field. *Journal of Physics: Condensed Matter*, 3(1):69, January 1991.

[3] Oleg A Starykh. Unusual Ordered Phases of Highly Frustrated Magnets: A Review. *Reports on Progress in Physics*, 78(5):052502, April 2015.

[4] B. Bernu, C. Lhuillier, and L. Pierre. Signature of Néel Order in Exact Spectra of Quantum Antiferromagnets on Finite Lattices. *Physical Review Letters*, 69(17):2590–2593, October 1992.

[5] B. Bernu, P. Lecheminant, C. Lhuillier, and L. Pierre. Néel Order versus Spin Liquid in Quantum Heisenberg Antiferromagnets on Triangular and Kagomé Lattices. *Physica Scripta*, 1993(T49A):192, January 1993.

[6] B. Bernu, P. Lecheminant, C. Lhuillier, and L. Pierre. Exact Spectra, Spin Susceptibilities, and Order Parameter of the Quantum Heisenberg Antiferromagnet on the Triangular Lattice. *Physical Review B*, 50(14):10048–10062, October 1994.

[7] Steven R. White and A. L. Chernyshev. Néel Order in Square and Triangular Lattice Heisenberg Models. *Physical Review Letters*, 99(12):127004, September 2007.

[8] Dag-Vidar Bauer and J. O. Fjærstad. Schrödinger-Boson Mean-Field Study of the  $J_1$ - $J_2$  Heisenberg Quantum Antiferromagnet on the Triangular Lattice. *Physical Review B*, 96(16):165141, October 2017.

[9] Francesco Ferrari and Federico Becca. Dynamical Structure Factor of the  $J_1$ - $J_2$  Heisenberg Model on the Triangular Lattice: Magnons, Spinons, and Gauge Fields. *Physical Review X*, 9(3):031026, August 2019.

[10] Shou-Shu Gong, W. Zhu, J.-X. Zhu, D. N. Sheng, and Kun Yang. Global Phase Diagram and Quantum Spin Liquids in a Spin- $\frac{1}{2}$  Triangular Antiferromagnet. *Physical Review B*, 96(7):075116, August 2017.

[11] Shijie Hu, W. Zhu, Sebastian Eggert, and Yin-Chen He. Dirac Spin Liquid on the Spin- $\frac{1}{2}$  Triangular Heisenberg Antiferromagnet. *Physical Review Letters*, 123(20):207203, November 2019.

[12] Yasir Iqbal, Wen-Jun Hu, Ronny Thomale, Didier Poilblanc, and Federico Becca. Spin Liquid Nature in the Heisenberg  $J_1$ - $J_2$  Triangular Antiferromagnet. *Physical Review B*, 93(14):144411, April 2016.

[13] P. A. Maksimov, Zhenyue Zhu, Steven R. White, and A. L. Chernyshev. Anisotropic-Exchange Magnets on a Triangular Lattice: Spin Waves, Accidental Degeneracies, and Dual Spin Liquids. *Physical Review X*, 9(2):021017, April 2019.

[14] S. N. Saadatmand and I. P. McCulloch. Detection and Characterization of Symmetry-Broken Long-Range Orders in the Spin- $\frac{1}{2}$  Triangular Heisenberg Model. *Physical Review B*, 96(7):075117, August 2017.

[15] Zhenyue Zhu and Steven R. White. Spin Liquid Phase of the  $S = \frac{1}{2}$   $J_1$ - $J_2$  Heisenberg Model on the Triangular Lattice. *Physical Review B*, 92(4):041105, July 2015.

[16] Zhenyue Zhu, P. A. Maksimov, Steven R. White, and A. L. Chernyshev. Topography of Spin Liquids on a Triangular Lattice. *Physical Review Letters*, 120(20):207203, May 2018.

[17] Yuesheng Li, Philipp Gegenwart, and Alexander A Tsirlin. Spin Liquids in Geometrically Perfect Triangular Antiferromagnets. *Journal of Physics: Condensed Matter*, 32(22):224004, March 2020.

[18] Ruidan Zhong, Shu Guo, Guangyong Xu, Zhijun Xu, and Robert J. Cava. Strong Quantum Fluctuations in a Quantum Spin Liquid Candidate with a Co-based Triangular Lattice. *Proceedings of the National Academy of Sciences*, 116(29):14505–14510, July 2019.

[19] N. Li, Q. Huang, X. Y. Yue, W. J. Chu, Q. Chen, E. S. Choi, X. Zhao, H. D. Zhou, and X. F. Sun. Possible Itinerant Excitations and Quantum Spin State Transitions in the Effective Spin-1/2 Triangular-Lattice Antiferromagnet  $\text{Na}_2\text{BaCo}(\text{PO}_4)_2$ . *Nature Communications*, 11(1):4216, August 2020.

[20] S. Lee, C. H. Lee, A. D. Hillier, Devashibhai T. Adroja, Ruidan Zhong, R. J. Cava, Z. H. Jang, and K.-Y. Choi. Temporal and Field Evolution of Spin Excitations in the Disorder-Free Triangular Antiferromagnet  $\text{Na}_2\text{BaCo}(\text{PO}_4)_2$ . *Physical Review B*, 103(2):024413, January 2021.

[21] Y. Y. Huang, D. Z. Dai, C. C. Zhao, J. M. Ni, L. S. Wang, B. L. Pan, B. Gao, Pengcheng Dai, and S. Y. Li. Thermal Conductivity of Triangular-Lattice Antiferromagnet  $\text{Na}_2\text{BaCo}(\text{PO}_4)_2$ : Absence of Itinerant Fermionic Excitations. [10.48550/arXiv.2206.08866](https://arxiv.org/abs/2206.08866), June 2022.

[22] Leonie Woodland, Ryutaro Okuma, J. Ross Stewart, Christian Balz, and Radu Coldea. From continuum excitations to sharp magnons via transverse magnetic field in the spin- $\frac{1}{2}$  Ising-like triangular lattice antiferromagnet  $\text{Na}_2\text{BaCo}(\text{PO}_4)_2$ . *Physical Review B*, 112(10):104413, September 2025.

[23] Jieming Sheng, Le Wang, Wenrui Jiang, Han Ge, Nan Zhao, Tiantian Li, Maiko Kofu, Dehong Yu, Wei Zhu, Jia-Wei Mei, Zhentao Wang, and Liusuo Wu. Continuum of Spin Excitations in an Ordered Magnet. *The Innovation*, 6(4), April 2025.

[24] Yuan Gao, Yu-Chen Fan, Han Li, Fan Yang, Xu-Tao Zeng, Xian-Lei Sheng, Ruidan Zhong, Yang Qi, Yuan Wan, and Wei Li. Spin Supersolidity in Nearly Ideal Easy-Axis Triangular Quantum Antiferromagnet  $\text{Na}_2\text{BaCo}(\text{PO}_4)_2$ . *npj Quantum Materials*, 7(1):89, September 2022.

[25] Junsen Xiang, Chuandi Zhang, Yuan Gao, Wolfgang Schmidt, Karin Schmalzl, Chin-Wei Wang, Bo Li, Ning Xi, Xin-Yang Liu, Hai Jin, Gang Li, Jun Shen, Ziyu Chen, Yang Qi, Yuan Wan, Wentao Jin, Wei Li, Peijie Sun, and Gang Su. Giant Magnetocaloric Effect

in Spin Supersolid Candidate  $\text{Na}_2\text{BaCo}(\text{PO}_4)_2$ . *Nature*, 625(7994):270–275, January 2024.

[26] T. Burnus, Z. Hu, H. H. Hsieh, V. L. J. Joly, P. A. Joy, M. W. Haverkort, Hua Wu, A. Tanaka, H.-J. Lin, C. T. Chen, and L. H. Tjeng. Local Electronic Structure and Magnetic Properties of  $\text{LaMn}_{0.5}\text{Co}_{0.5}\text{O}_3$  Studied by x-Ray Absorption and Magnetic Circular Dichroism Spectroscopy. *Physical Review B*, 77(12):125124, March 2008.

[27] C. Wellm, W. Roscher, J. Zeisner, A. Alfonsov, R. Zhong, R. J. Cava, A. Savoyant, R. Hayn, J. van den Brink, B. Büchner, O. Janson, and V. Kataev. Frustration Enhanced by Kitaev Exchange in a  $\tilde{J}_{\text{eff}} = \frac{1}{2}$  Triangular Antiferromagnet. *Physical Review B*, 104(10):L100420, September 2021.

[28] Banasree S. Mou, Xinshu Zhang, Li Xiang, Yuanyuan Xu, Ruidan Zhong, Robert J. Cava, Haidong Zhou, Zhigang Jiang, Dmitry Smirnov, Natalia Drichko, and Stephen M. Winter. Comparative Raman Scattering Study of Crystal Field Excitations in Co-based Quantum Magnets. *Physical Review Materials*, 8(8):084408, August 2024.

[29] Ghulam Hussain, Jianbo Zhang, Man Zhang, Lalit Yadav, Yang Ding, Changcheng Zheng, Sara Haravifard, and Xiawa Wang. Experimental Evidence of Crystal-Field, Zeeman-splitting, and Spin-Phonon Excitations in the Quantum Supersolid  $\text{Na}_2\text{BaCo}(\text{PO}_4)_2$ . *Physical Review B*, 111(15):155129, April 2025.

[30] T. I. Popescu, N. Gora, F. Demmel, Z. Xu, R. Zhong, T. J. Williams, R. J. Cava, G. Xu, and C. Stock. Zeeman Split Kramers Doublets in Spin-Supersolid Candidate  $\text{Na}_2\text{BaCo}(\text{PO}_4)_2$ . *Physical Review Letters*, 134(13):136703, April 2025.

[31] Arata Tanaka and Takeo Jo. Resonant 3d, 3p and 3s Photoemission in Transition Metal Oxides Predicted at 2p Threshold. *Journal of the Physical Society of Japan*, 63(7):2788–2807, July 1994.

[32] F.M.F. De Groot. X-Ray Absorption and Dichroism of Transition Metals and Their Compounds. *Journal of Electron Spectroscopy and Related Phenomena*, 67(4):529–622, August 1994.

[33] T. Burnus, Z. Hu, M. W. Haverkort, J. C. Cezar, D. Flahaut, V. Hardy, A. Maignan, N. B. Brookes, A. Tanaka, H. H. Hsieh, H.-J. Lin, C. T. Chen, and L. H. Tjeng. Valence, Spin, and Orbital State of Co Ions in One-Dimensional  $\text{Ca}_3\text{Co}_2\text{O}_6$  : An x-Ray Absorption and Magnetic Circular Dichroism Study. *Physical Review B*, 74(24):245111, December 2006.

[34] H.-J. Lin, Y. Y. Chin, Z. Hu, G. J. Shu, F. C. Chou, H. Ohta, K. Yoshimura, S. Hébert, A. Maignan, A. Tanaka, L. H. Tjeng, and C. T. Chen. Local Orbital Occupation and Energy Levels of Co in  $\text{Na}_x\text{CoO}_2$  : A Soft x-Ray Absorption Study. *Physical Review B*, 81(11):115138, March 2010.

[35] Y. Y. Chin, Z. Hu, H.-J. Lin, S. Agrestini, J. Weinan, C. Martin, S. Hébert, A. Maignan, A. Tanaka, J. C. Cezar, N. B. Brookes, Y.-F. Liao, K.-D. Tsuei, C. T. Chen, D. I. Khomskii, and L. H. Tjeng. Spin-Orbit Coupling and Crystal-Field Distortions for a Low-Spin 3d<sup>5</sup> State in  $\text{BaCoO}_3$ . *Physical Review B*, 100(20):205139, November 2019.

[36] A. J. Achkar, T. Z. Regier, H. Wadati, Y.-J. Kim, H. Zhang, and D. G. Hawthorn. Bulk Sensitive X-Ray Absorption Spectroscopy Free of Self-Absorption Effects. *Physical Review B*, 83(8):081106, February 2011.

[37] A. J. Achkar, T. Z. Regier, E. J. Monkman, K. M. Shen, and D. G. Hawthorn. Determination of Total X-Ray Absorption Coefficient Using Non-Resonant x-Ray Emission. *Scientific Reports*, 1(1):182, December 2011.

[38] Huang-Ming Tsai, Huang-Wen Fu, Chang-Yang Kuo, Liang-Jen Huang, Chang-Sheng Lee, Chih-Yu Hua, Kai-Yang Kao, Hong-Ji Lin, Hok-Sum Fung, Shih-Chun Chung, Chun-Fu Chang, Ashish Chainani, Liu Hao Tjeng, and Chien-Te Chen. A Submicron Soft X-Ray Active Grating Monochromator Beamline for Ultra-High Resolution Angle-Resolved Photoemission Spectroscopy. *AIP Conference Proceedings*, 2054(1):060047, January 2019.

[39] M. M. Ferreira-Carvalho, S. Rößler, C. F. Chang, Z. Hu, S. M. Valvidares, P. Gargiani, M. W. Haverkort, Prashanta K. Mukharjee, P. Gegenwart, A. A. Tsirlin, and L. H. Tjeng. Trigonal Distortion in the Kitaev Candidate Honeycomb Magnet  $\text{BaCo}_2(\text{AsO}_4)_2$ . *Physical Review B*, 112:125135, September 2025.

[40] M. W. Haverkort, M. Zwierzycki, and O. K. Andersen. Multiplet Ligand-Field Theory Using Wannier Orbitals. *Physical Review B*, 85(16):165113, April 2012.

[41] M. W. Haverkort, G. Sangiovanni, P. Hansmann, A. Toschi, Y. Lu, and S. Macke. Bands, Resonances, Edge Singularities and Excitons in Core Level Spectroscopy Investigated within the Dynamical Mean-Field Theory. *Europhysics Letters*, 108(5):57004, December 2014.

[42] Y. Lu, M. Höppner, O. Gunnarsson, and M. W. Haverkort. Efficient Real-Frequency Solver for Dynamical Mean-Field Theory. *Physical Review B*, 90(8):085102, August 2014.

[43] Quanty version 0.81. <https://www.quanty.org>.

[44] R. D. Cowan. *The Theory of Atomic Structure and Spectra*. University of California Press, September 1981.

[45] A. E. Bocquet, T. Mizokawa, K. Morikawa, A. Fujimori, S. R. Barman, K. Maiti, D. D. Sarma, Y. Tokura, and M. Onoda. Electronic Structure of Early 3d-Transition-Metal Oxides by Analysis of the 2p Core-Level Photoemission Spectra. *Physical Review B*, 53(3):1161–1170, January 1996.

[46] S. I. Csiszar, M. W. Haverkort, Z. Hu, A. Tanaka, H. H. Hsieh, H.-J. Lin, C. T. Chen, T. Hibma, and L. H. Tjeng. Controlling Orbital Moment and Spin Orientation in CoO Layers by Strain. *Physical Review Letters*, 95(18):187205, October 2005.

[47] N. Hollmann, Z. Hu, T. Willers, L. Bohatý, P. Becker, A. Tanaka, H. H. Hsieh, H.-J. Lin, C. T. Chen, and L. H. Tjeng. Local Symmetry and Magnetic Anisotropy in Multiferroic  $\text{MnWO}_4$  and Antiferromagnetic  $\text{CoWO}_4$  Studied by Soft X-Ray Absorption Spectroscopy. *Physical Review B*, 82(18):184429, November 2010.

[48] Klaus Koepernik and Helmut Eschrig. Full-Potential Nonorthogonal Local-Orbital Minimum-Basis Band-Structure Scheme. *Physical Review B*, 59(3):1743–1757, January 1999.

[49] FPLO version 21.00. <https://www.fplo.de>.

[50]  $U_{dd} = 6.5$  eV,  $U_{pd} = 8.2$  eV, charge energy transfer  $\Delta = 6.5$  eV, SOC = 0.066 eV, ionic crystal field  $10Dq^{ion} = 0.395$  eV,  $D_{trig}^{ion} = 8$  meV, hybridization  $V(e_g^\sigma) = 2.45$  eV,  $V(e_g^\pi) = 1.31$  eV,  $V(a_{1g}) = 1.29$  eV (this hybridization values are then scaled to 83%), ligand crystal field = 0.693 eV. Slater integrals were reduced to 80% of the Hartree-Fock values.

[51] M. van Veenendaal, E. H. T. Poldi, L. S. I. Veiga, P. Ben-cok, G. Fabbris, R. Tartaglia, J. L. McChesney, J. W. Freeland, R. J. Hemley, H. Zheng, J. F. Mitchell, J.-Q. Yan, and D. Haskel. Electronic Structure of Co 3d States in the Kitaev Material Candidate Honeycomb Cobaltate  $\text{Na}_3\text{Co}_2\text{SbO}_6$  Probed with X-Ray Dichroism. *Physical Review B*, 107(21):214443, June 2023.

[52] Gordon A. Bain and John F. Berry. Diamagnetic Corrections and Pascal's Constants. *Journal of Chemical Education*, 85(4):532, April 2008.

[53] S. Agrestini, C.-Y. Kuo, K. Chen, Y. Utsumi, D. Mikhailova, A. Rogalev, F. Wilhelm, T. Förster, A. Matsumoto, T. Takayama, H. Takagi, M. W. Haverkort, Z. Hu, and L. H. Tjeng. Probing the  $J_{\text{Eff}} = 0$  Ground State and the Van Vleck Paramagnetism of the Ir  $5^+$  Ions in Layered  $\text{Sr}_2\text{Co}_{0.5}\text{Ir}_{0.5}\text{O}_4$ . *Physical Review B*, 97(21):214436, June 2018.

[54] Miguel Carvalho. Direct Evidence of a Near-Ideal  $J_{\text{eff}} = 1/2$  Ground State in Triangular-Lattice  $\text{Na}_2\text{BaCo}(\text{PO}_4)_2$ , <https://doi.org/10.17617/3.xe7bis>, 2025.